RodA Promotes Intestinal Colonization by Group B *Streptococcus*

Authors:

Michelle J. Vaz[a#], Sanjana Sankaran[a#], Molly E. Sharp[b], Emily Dembinski[b], Adam J. Ratner[a,b]

#Equal authorship contribution

Affiliations:

[a] Department of Pediatrics, NYU Grossman School of Medicine, New York, New York, USA

[b] Department of Microbiology, NYU Grossman School of Medicine, New York, New York, USA

*Address correspondence to Adam J. Ratner, adam.ratner@nyulangone.org

Running title: Conditional essentiality of *rodA* in GBS intestinal colonization

Key Words: *Streptococcus agalactiae (*Group B *Streptococcus), rodA,* gastrointestinal colonization, murine model.

Abstract:

Background. Group B *Streptococcus* (GBS) intestinal colonization is critical for the pathogenesis of late-onset (LO) disease in infants. Using a murine model, we explore the role of *rodA*, which encodes a peptidoglycan polymerase RodA, belonging to the Shape, Elongation, Division, and Sporulation (SEDS) family that participates in peptidoglycan synthesis and maintenance of cell wall integrity.

Methods. We investigated the contribution of *rodA* to GBS gastrointestinal (GI) colonization using a wild-type strain (A909 WT) and an isogenic in-frame deletion mutant of *rodA* (A909Δ*rodA*). Morphological differences between the two strains were examined by transmission electron microscopy (TEM), and the contribution of *rodA* to GI colonization was assessed in a murine model through monocolonization and cocolonization experiments. We evaluated the growth of the mutant strain under intestinal physiological stress conditions and characterized its interactions with host epithelial cells in vitro.

Results. A909Δ*rodA* showed a unique chaining/aggregation phenotype compared to the A909 WT strain, with the presence of capsule confirmed via TEM and immunoblotting. In murine cocolonization experiments, A909 WT outcompeted A909Δ*rodA*; however, monocolonization experiments exhibited comparable colonization and bacterial burden across the GI tract. In vitro experiments revealed impaired growth in bile and an increase in adhesion to intestinal epithelial cells by the Δ*rodA* mutant.

Conclusion(s): *rodA* plays a role in GBS intestinal colonization. Deletion of *rodA* increases sensitivity to gastrointestinal stressors in vitro and causes a pronounced defect in competition in vivo, suggesting that the presence of *rodA* increases the fitness of GBS in the gut.

45 **Introduction**

46 *Streptococcus agalactiae* (Group B *Streptococcus* [GBS]) is a leading etiology of neonatal
47 infection (1). Implementation of intrapartum antibiotic prophylaxis has markedly reduced the
48 incidence of early onset (EO) infection (occurring ≤ 7 days of life) (2, 3). However, rates of
49 maternal rectovaginal colonization persist, and the incidence of late onset (LO) infection
50 (occurring ≥7 days of life) remains unchanged, making LO disease the predominant form of
51 invasive GBS infection in infants (4, 5). Recent work has shown the incidence of LO disease
52 amongst a cohort of extremely preterm infants (< 28 weeks) as 8.47/1000 infants, nearly 30
53 times the national incidence of all neonates (6). LO disease has an overall case fatality rate of 4-
54 12%, with the rates in preterm infants being twice that of term infants (3, 7). The sequelae of LO
55 disease include significant neurodevelopmental impairment in survivors, adding to the morbidity
56 burden (2, 8-11).

57 Prior studies have demonstrated that gastrointestinal (GI) colonization by GBS in infants is a
58 fundamental precursor for LO infection (12, 13). Understanding how GBS establishes itself in
59 the bacterial community of the intestinal tract can uncover mechanisms that contribute to the
60 pathogenesis of LO disease. Our group recently showed the contribution of capsular
61 polysaccharide, an important GBS virulence factor, to GI fitness and colonization in a murine
62 model of GBS intestinal colonization (14). Hence, robust animal models facilitate examination of
63 bacterial factors that augment or inhibit GI colonization.

64 In this report, we explore the role of GBS *rodA*, a gene that encodes the peptidoglycan
65 polymerase RodA, which belongs to the SEDS family of proteins. RodA, through its role as a
66 glycosyltransferase and in conjunction with penicillin-binding proteins (PBPs), is responsible for
67 peptidoglycan synthesis, which is vital for cell wall integrity and responsible for bacterial

68 survival under environmental stress (15, 16). It is known to contribute to bile salt resistance by
69 GBS (17). In this report, we generated an in-frame deletion of *rodA* in the GBS A909
70 background using CRISPR-Cas12a mutagenesis and studied its impact on the cell wall and
71 capsule. We analyzed its response to intestinal physiological stressors and determined its role in
72 a postnatal murine model of GI colonization.
73
74 **Methods**
75 **Bacterial Strains and Growth Conditions.** GBS strain A909 (serotype Ia, ST7) and its
76 derivatives were grown to stationary phase at 37°C in tryptic soy (TS) broth supplemented with 5
77 µg/ml erythromycin as needed for selection. *Escherichia coli* strain DH5α was grown at 37°C,
78 shaking in Luria-Bertani (LB) medium supplemented with 300 µg/ml erythromycin when needed
79 for selection.
80 **Construction of the GBS *rodA* deletion mutant and its complemented control strain.** The
81 *rodA* deletion mutant was created via a Cas12a-based platform as previously described
82 (18). Briefly, a Cas12a-compatible genomic target site in the *rodA* gene was identified using the
83 CRISPick server hosted by the Broad Institute (19). After selecting a target sequence, we
84 designed ssDNA oligonucleotides and annealed them to make a dsDNA protospacer. The
85 protospacer was then cloned into pGBSedit that had been linearized with Esp3I. The pGBSedit
86 plasmid encodes *cas12a*, regulated by a $P_{xyl/tet}$ promoter, that responds to the presence of
87 anhydrotetracycline (aTC). Primer pairs were used to amplify upstream and downstream
88 homology arms flanking *rodA*. These fragments were cloned into pGBSedit linearized with XhoI
89 using Gibson assembly. Following transformation into *E. coli*, plasmids were verified via PCR
90 and whole-plasmid sequencing. Sequenced plasmids were transformed into electrocompetent

91 GBS and successful transformants were confirmed by colony PCR (cPCR). Transformants were
92 then subcultured in 10 mL TS + erythromycin (5 µg/mL) and allowed to grow at 37 °C for 6–8
93 hours. Subsequently, the cultures were subjected to aTC induction (500 ng/ml), resulting in
94 strong selection against WT strains and for homology-driven recombination mutants (20). cPCR
95 was used once again to confirm deletion mutants. Once confirmed, colonies were inoculated into
96 40 mL TS broth and grown overnight at 37°C. After a second passage of overnight growth in
97 40 mL of TS broth, 1:10,000 and 1:100,000 dilutions were plated on TS agar plates. The next
98 day colonies were dual patched onto TS and TS + erythromycin (5 µg/mL) agar plates to detect
99 cured clones. All constructs were confirmed by PCR and sequencing. We complemented the
100 *rodA* gene deletion by using the pGBScomp High plasmid (A909Δ*rodA*+pGBScomp
101 High::*rodA)* (18). Briefly, pGBScomp High plasmid was linearized via SalI restriction digest,
102 and the *rodA* gene was PCR amplified. The two products were Gibson assembled and
103 transformed into *E. coli* followed by confirmation by sequencing. Electrocompetent GBS was
104 transformed with the plasmid and confirmed using cPCR. Primers used in the construction of the
105 mutant and complemented strain are listed in **(Supplemental Table 1).** The transposon *rodA*
106 mutant (A909 *rodA::Himar1*) was used from a large-scale GBS indexed library of *Himar1* mini-
107 transposon mutant strains, containing interruptions of 878 genes and 253 intergenic regions, each
108 with an erythromycin resistance cassette (21).
109 **Microscopy and Staining.**
110 **Gram Stain.** WT A909 and A909Δ*rodA* strains were grown overnight in TS broth at 37 °C.
111 Cells were harvested by centrifugation (4,000 rpm, 10 min), washed once with Dulbecco's
112 phosphate-buffered saline (DPBS), and resuspended in DPBS. Smears were prepared on clean
113 glass slides, heat-fixed, and subjected to Gram staining using the standard four-step protocol:

114 crystal violet (1 min), Gram's iodine (1 min), decolorization with 95% ethanol (10–15 s), and
115 counterstaining with safranin (30 s), as previously described (22). Slides were rinsed gently with
116 distilled water between each step and air-dried. Stained preparations were examined by light
117 microscopy (1000×, oil immersion). Brightfield images were acquired using a Zeiss Axio
118 Observer microscope equipped with a 63×/1.4 oil immersion objective.
119 **Colony immunoblotting.** Overnight cultures of WT A909, A909Δ*rodA* and A909Δ*cpsE*
120 (acapsular control) were spread on CHROMagar plates. Colonies were counted to identify plates
121 with 20–200 colonies for subsequent immunoblotting. Plates were briefly overlaid with
122 nitrocellulose membranes (Amersham) to allow adherence of GBS material to the membrane.
123 Membranes were blocked in 3% bovine serum albumin (BSA) in DPBS (blocking solution) for 1
124 hour. Blots were then transferred to type Ia *Streptococcus* group B type antisera (Statens Serum
125 Institut) and incubated for 30 minutes with gentle shaking. Type Ia antiserum was diluted
126 1:2,000 in the blocking solution. Blots were then washed three times in DPBS. Blots were
127 incubated in horseradish peroxidase (HRP)-conjugated goat anti-rabbit secondary antibody
128 (Pierce) diluted 1:1,000 in blocking solution for 2 hours. Blots were washed three times in DPBS
129 and stained using a 3,3′-diaminobenzidine tetrahydrochloride substrate kit (Abcam).
130 **Electron microscopy.** Overnight cultures were pelleted for 5 min at 4,000 rpm. Samples were
131 processed and imaged by the NYU Microscopy Laboratory as previously described with
132 modifications (23). In brief, bacteria were resuspended in 1 mL LRR (Lysine-Ruthenium Red-
133 Osmium) fixative solution (1 mL fixation solution per sample: 0.5 mL 0.15% ruthenium red, 125
134 µL 16% formaldehyde, 100 µL 25% glutaraldehyde solution, 0.0155 g lysine acetate; fill with
135 distilled water to 1 mL). The cells were fixed on ice for 20 min, washed two times with 0.1M
136 sodium cacodylate buffer (0.1M cacodylate, 0.01M $CaCl_2$, 0.01M $MgCl_2$, 0.09M sucrose, pH

137 6.9) containing 0.075% ruthenium red and fixed in the fixation solution without lysine acetate for
138 2 hrs on ice. After washing three times with 0.1M sodium cacodylate buffer containing 0.075%
139 ruthenium red for 5 min each, the cells were postfixed in 1% osmium tetroxide (OsO_4) with
140 0.075% ruthenium red in 0.1M sodium cacodylate buffer for 1h on ice, washed three times with
141 0.1M sodium cacodylate buffer with 0.075% ruthenium red for 5 min each, then embedded with
142 2% agar and *en block* stained with 0.5% uranyl acetate aqueous solution overnight at 4ºC. The
143 samples were washed with distilled water, dehydrated in a graded ethanol series (30%: 50%:
144 75%, 85%: 90%:100%:100%) on ice, infiltrated and embedded with LR White resin (Electron
145 Microscopy Sciences, PA) at 55ºC. Thin sections were cut using Leica UC6 ultramicrotome,
146 collected on 200 mesh copper grids (Ted, Pella Inc. CA), and stained with 4% aqueous uranyl
147 acetate for 5 minutes. Stained grids were examined under JEOL1400 Flash transmission electron
148 microscope (Japan) and photographed with a Gatan Rio 16 camera (Gatan Inc. Pleasanton, CA).
149 **GI colonization model.** All experiments were performed in accordance with the NYU Grossman
150 School of Medicine's Institutional Animal Care and Use Committee (IACUC). These
151 experiments were conducted as previously described (24). Adult male and female C57BL/6J
152 mice (8–12 weeks) were purchased from Jackson Laboratories (Bar Harbor, Maine), given at
153 least 3 days to acclimate to the local facility, and mated as pairs and trios. Dams were monitored
154 for the birth of litters, and animals aged 12–14 days (preweaning) were used for colonization.
155 Two cohorts were used for cocolonization: one for cocolonization with A909 WT and
156 A909Δ*rodA* strains and the other using A909 WT and A909 *rodA::Himar1*. Bacterial cultures
157 were grown, centrifuged and resuspended in sterile DPBS, and a 1:1 mixture was made of the
158 resuspended strains to be competed. Animals were orally fed using a sterile feeding tube with
159 10^8 colony forming units (CFUs) of GBS resuspended in 50 µL of DPBS. Animals remained

160 housed with their biological dams and were monitored daily for signs of illness and mortality. At
161 predetermined time points (7- and 14-days post-infection), animals were euthanized, and the GI
162 tract was harvested. Each portion (small intestine, cecum, and colon) was homogenized. Serial
163 dilutions were plated on CHROMagar StrepB for the enumeration of GBS CFUs. In addition,
164 dilutions were spread on CHROMagar plates, with and without antibiotic selection
165 (erythromycin), for differentiation between A909 WT and A909 *rodA::Himar1*. A909 WT and
166 A909Δ*rodA* were differentiated by picking individual colonies for screening using cPCR. For the
167 monocolonization model, bacterial cultures were grown overnight to stationary phase and the
168 optical densities of the two strains were normalized. Cultures were then centrifuged and
169 resuspended in sterile DPBS to a final concentration of 10^9 CFU/mL. Animals were orally fed
170 using a sterile feeding tube with 10^8 CFU of GBS resuspended in 50 µL of DPBS and remained
171 with their biologic, non-colonized dam. The animals were monitored daily for signs of illness
172 and mortality. At predetermined time points (3-, 7-, and 14-days post-infection), animals were
173 euthanized, and the GI tract was harvested. Each portion (small intestine, cecum, and colon) was
174 homogenized, and serial dilutions were plated for enumeration of GBS CFUs on CHROMagar.
175 **Colony differentiation using cPCR.** Bacterial colonies recovered from the cocolonization
176 experiment were screened for the presence or absence of *rodA* using cPCR. We selected ~20
177 colonies per site per mouse (~100 colonies per site), from organ dilutions that had been spread
178 on CHROMagar plates. Selected colonies were patched on TS plates overnight, then resuspended
179 in 20 µL of PBS, of which 2 µL was used as a template in a 25 µL PCR reaction containing
180 OneTaq 2xMM, forward and reverse check primers **(Supplementary Table 1)** specific for the
181 flanking region of the *rodA* gene and RNAse-free water. PCR was conducted using an annealing

182 temperature of 54°C and 2-minute extension. Products were run on 1% agarose gel. Amplicon
183 length was compared to A909 WT and A909Δ*rodA* controls to confirm genotype.
184 Competitive index for cocolonization experiments was calculated as: (CFU strain 1
185 recovered/CFU strain 1 inoculated)/(CFU strain 2 recovered/CFU strain 2 inoculated) and log-
186 transformed for calculation of geometric mean and 95% confidence interval (CI) for each GI site.
187 **Growth rate analysis under physiological stressors.** To investigate bacterial growth rate under
188 acidic pH, bile, and lysozyme conditions, overnight cultures were assayed as described
189 previously (17, 25, 26). TS broth was adjusted to pH 6.0 and 5.0 using sterile 1 N HCl. TS broth
190 was prepared and autoclaved, cooled to room temperature (or 37 °C for temperature-matched
191 readings), and stirred aseptically while titrating with sterile 1 N HCl. pH was monitored with a
192 calibrated pH meter until 6.00 ± 0.05 and 5.00 ± 0.05 was reached. Media were re-checked after
193 10 min equilibration, dispensed, and used the same day. Control medium (pH 7.0) was handled
194 identically without acid addition. Bile concentrations (5 mg/ml and 10 mg/ml) from a stock
195 concentration of 200 mg/ml and lysozyme concentration of 14 mg/ml from a stock concentration
196 of 100 mg/ml (made in DPBS) were prepared in TSB and sterilized prior use. Lysozyme
197 concentration was determined through preliminary testing of multiple concentrations, with the
198 final concentration selected to yield ~50% killing in the WT strain (LD_{50}) (**Supplemental**
199 **Figure S1)**. Overnight cultures were diluted to an OD_{600} of 0.05 in TS broth, 150 µL of each
200 culture was added to a 96-well plate in three technical replicates. Media-only wells served as
201 negative controls, and all readings were normalized to the negative control. Growth curve assays
202 were performed using the BioTek LogPhase 600 Microbiology Reader for 24 hours at 37 °C,
203 with readings taken every 20 minutes.

204 **Biofilm Assay.** Biofilm assays were performed as previously described (27). Briefly, overnight
205 bacterial cultures grown in TSB were diluted to an OD_{600} of 0.05 in Todd Hewitt Broth (THB)
206 with 1% glucose, incubated for 24 hours at 37°C with 5% CO_2 in 12 wells, flat bottom tissue
207 culture plates. Staining was performed the next day using 0.5% crystal violet, solubilized with
208 30% glacial acetic acid and 100uL of samples were transferred to 96 well cell culture plates for
209 readings. Spectra Max M3 was used to obtain readings at OD_{540}. Biofilms under stress conditions
210 were tested by diluting bacteria in THB 1% glucose with the relevant stress media as described
211 above.
212 **Tissue culture assays:** The human intestinal Caco-2 cell line (ATCC HTB-37; colorectal
213 adenocarcinoma) was seeded in 24-well plates at a density of 1 x 10^4 cells per well in Eagle's
214 Minimum Essential Medium (EMEM, ATCC 30-2003) supplemented with 20% (vol/vol) fetal
215 bovine serum (FBS, HyClone Cytiva, Marlborough, MA) and 1% penicillin-streptomycin
216 (Pen/Strep, 10,000 U/mL, Gibco, USA) and cultured at 37°C in a humidified 5% CO_2 incubator
217 (28). The T84 colonic epithelial cell line (ATCC CCL-248) were cultivated in Dulbecco's
218 Modified Eagle's Medium and Ham F-12 medium (DMEM: F-12, ATCC 30-2006)
219 supplemented with 10% FBS and 1% Pen/Strep (29). For adherence assays, bacterial strains
220 were grown overnight in TS broth. On the day of the assay, bacterial strains were diluted to an
221 OD_{600} of 0.1 and grown until mid-log phase. Caco-2 and T84 cells were grown to confluence in
222 12-well and 24-well tissue culture-treated plates (Corning). One hour prior to the assay, cell
223 culture media was replaced with antibiotic - and serum-free media. Cells were washed three
224 times with DPBS prior to infection. Bacteria were washed three times with DPBS and then
225 resuspended in DMEM: F-12 or EMEM, depending on the cell type and added to cells at a
226 multiplicity of infection (MOI) of 10. Adhesion was assessed after 45 minutes. Cells were

227 washed six times with DPBS, removed from plates with trypsin-EDTA, and lysed with 0.1%
228 saponin (30). Lysates were serially diluted and plated on TS agar (TSA) plates to quantify the
229 number of adherent CFU. Adherence was calculated as: (total CFU recovered/total CFU of
230 original inoculum) × 100%. For invasion assays, bacterial strains were prepared in the same
231 manner as for adherence. Following three washes, bacteria was added to each well, and plates
232 were incubated for 150 minutes to allow invasion. Plates were then washed six times to remove
233 non-adherent bacteria. Antibiotic-containing culture media was prepared by adding gentamicin
234 and penicillin from prepared stocks of 50 mg/mL each with a final concentration of 100 μg/mL
235 gentamicin and 5 μg/mL penicillin. Plates were incubated for an additional 2 hours with
236 antibiotic media, after which invasion capacity was assessed using the same procedures
237 described for adherence.

238 **Statistical Analysis.** Statistics were calculated using GraphPad Prism 10.5.0 software.
239 Colonization rates between the A909 WT and A909Δ*rodA* strains were compared using Fisher's
240 exact test. Bacterial burden comparison between the A909 WT and A909Δ*rodA* strains at
241 different GI tract sites were compared using two-way repeated measures ANOVA with Sidak's
242 multiple comparisons post-test. Biofilm formation under different stressors was evaluated using
243 two-way ANOVA with the Tukey multiple comparisons test. Tissue culture adhesion and
244 invasion assays were compared using Mann-Whitney U test.

245 **Results**

246 **Structural characterization of GBS A909Δ*rodA*:** To characterize the structural contribution of
247 *rodA*, we generated an in-frame deletion mutant (A909Δ*rodA)* using the Cas12a mutagenesis
248 system as previously described (18). Overnight growth showed pronounced sedimentation of the
249 A909Δ*rodA* compared to the A909 WT strain and complemented A909Δ*rodA*+pGBScomp

250 High::*rodA*, although no significant differences were noted in growth rate **(Supplemental**
251 **Figure S2, Figure 4A)**. Gram staining revealed a typical streptococcal morphology, with chains
252 of cocci in the WT strain whereas the A909Δ*rodA* strain displayed a marked aggregation
253 phenotype, with cells forming dense clusters versus discrete chains **(Figure 1A).** Since GBS
254 capsule is anchored to the peptidoglycan layer, we assessed capsule presence to determine if
255 *rodA* played a role in its production (31). Colony immunoblotting using a capsule-specific
256 antibody detected capsule on both the A909 WT and A909 Δ*rodA* strains in contrast to the
257 A909Δ*cpsE,* which did produce capsule (**Figure 1B).** In addition, we confirmed the presence of
258 capsule production in the A909Δ*rodA* strain by latex agglutination (**Figure 1C).** Transmission
259 electron microscopy did not reveal obvious abnormalities in morphology or envelope appearance
260 in the A909Δ*rodA* strain compared to the A909 WT strain **(Figure 1D)**. These findings suggest a
261 phenotype with chaining and aggregation in the A909Δ*rodA* strain, without detectable changes in
262 capsule expression or obvious structural defects.

263 ***rodA* provides a competitive advantage in GI colonization.** To assess the contribution of *rodA*
264 in GI colonization, we initially employed a *rodA* transposon mutant (A909 *rodA::Himar1*). In
265 cocolonization experiments, we noted that A909 WT outcompeted A909 *rodA::Himar1,* with
266 geometric mean competitive indices 6.62, 95% CI [0.85, 53.1] and 4.19, 95% CI [1.70, 10.35] in
267 the small intestine; 7.67, 95% CI [1.69, 34.8] and 45.78, 95% CI [10.38, 201.7] in the cecum,
268 and 7.5, 95% CI [1.68, 33.76] and 49.82, 95% CI [17.72, 140.1] in the colon, at 7 and 14 days
269 respectively indicating a competitive advantage in vivo **(Supplemental Figure S3).** Based on
270 these pilot findings, we used the in-frame deletion mutant (A909Δ*rodA*) to validate the in vivo
271 phenotype. Preweaning mice (12–14 days) were orally infected in cocolonization experiments as
272 described (24). Animals cocolonized with the A909 WT and A909Δ*rodA* strains were monitored

273 for signs of illness and survival until 7 days post infection. There was 100% survival in this
274 cohort at the experimental endpoint of 7 days, at which point animals were euthanized and the GI
275 tract harvested **(Figure 2A)**. Colonies recovered from the small intestine, cecum, and colon were
276 analyzed using cPCR to determine the ratio of A909 WT to A909Δ*rodA* **(Supplemental Figure**
277 **4)**. In the small intestine and cecum, the A909 WT strain outcompeted the A909Δ*rodA* strain
278 with a geometric mean competitive index of 40, 95% CI [40, 40] at 7 days post-colonization,
279 denoting no variation across replicates, as all tested colonies were A909 WT **(Figure 2B)**. In the
280 colon, we calculated a geometric mean of 34.47, 95% CI [22.8, 52.11] **(Figure 2B)**. These
281 findings suggest a sustained competitive advantage of the A909 WT strain over the A909Δ*rodA*
282 strain throughout the GI tract.

283 ***rodA* is dispensable for intestinal colonization in the absence of competition.** We next
284 assessed the role of *rodA* in monocolonization. In longitudinal experiments across multiple
285 cohorts, pre-weaning mice were orally infected with either the A909 WT strain or the
286 A909Δ*rodA* strain. These animals were longitudinally monitored for signs or illness/mortality,
287 with cohorts euthanized at days 3, 7 or 14. We noted equivalent bacterial colonization between
288 the A909 WT and A909Δ*rodA* strains throughout the GI tract at all 3 time points **(Figure 3 A, C,**
289 **E)**. On further assessment, we noted comparable bacterial burden throughout the GI tract, except
290 in the colon at day 3 and day 7 post colonization, where the A909 WT strain had a higher median
291 colonization density than the A909Δ*rodA* strain **(Figure 3 B, D, F)**. There was an overall
292 decrease in bacterial burden at day 14 post infection, across strains **(Figure 3F)**. Taken together,
293 we note that A909Δ*rodA* demonstrated adequate colonization efficacy in monocolonization
294 experiments; however, it was outcompeted by the A909 WT strain in cocolonization. This

295 suggests that *rodA* may not be strictly essential for establishment of intestinal colonization but
296 may confer a selective advantage under competitive pressure.

297 **Investigating the role of *rodA* in response to intestinal physiological stress:** To further
298 characterize the role of *rodA* in the GI tract, we explored bacterial growth in vitro in the presence
299 of physiological gastrointestinal stress conditions. We monitored growth of A909 WT,
300 A909Δ*rodA* and complemented strain (A909Δ*rodA*+pGBScomp High::*rodA*) in TSB with acidic
301 pH in the range of 5.0-7.34, bile concentrations of 5 mg/mL and 10 mg/mL, and lysozyme (14
302 mg/ml). The growth of all three strains was unaffected by a pH of 6, however there was an
303 overall decrease in growth rate and bacterial mass at a pH of 5 for all strains **(Figure 4B, C)**. The
304 growth of A909Δ*rodA* was markedly inhibited in both bile salt concentrations, while the WT
305 strain grew adequately, and the complemented strain exhibited partial restoration of growth at
306 both bile concentrations **(Figure 4D, E)**. Short term lysozyme exposure resulted in ~50%
307 reduction in viability of A909 WT (**Supplemental Figure S1),** however we noted no significant
308 difference in long term growth in both strains in the presence of lysozyme **(Figure 4F).** In all
309 assays, the complemented strain showed a delay in entry into log phase, likely due to growth
310 under antibiotic selection pressure. Together these findings suggest that *rodA* is not required for
311 survival under acid stress and does not contribute to lysozyme resistance in long term assays, but
312 it is required for optimal growth in the presence of bile salts.

313 ***rodA* influences bacterial surface contact to epithelial surfaces and modulates host**
314 **interactions**: As biofilm formation and adhesion to host epithelial surfaces are both important
315 for gastrointestinal persistence, we next examined whether deletion of *rodA* altered these
316 phenotypes. We assessed the formation of biofilm in A909 WT and A909Δ*rodA* strains after
317 exposure to acidic media, lysozyme and bile. At pH 6.0, no difference was noted in biofilm

318 production between the WT and mutant strains **(Figure 5A)**. At pH 5.0, the A909Δ*rodA* strain
319 exhibited a non-significant decrease in biofilm production compared to its control (standard
320 media, pH 7.34) **(Figure 5B)**. On exposure to lysozyme, we noted an increase in biofilm
321 formation by the A909 WT strain that was not seen in the A909Δ*rodA* strain **(Figure 5C)**. The
322 presence of bile salts decreased the formation of biofilm in both the WT and mutant strains when
323 compared to their respective controls **(Figure 5D, E)**. To understand the surface associated
324 behavior of *rodA* at epithelial barriers, we performed adherence and invasion assays using
325 differentiated Caco-2 intestinal epithelial cells and T84 colonic epithelial cell lines, in an in vitro
326 model. We evaluated if the adherence and/or invasion to epithelial cells by GBS depended on
327 *rodA*. Adherence assays showed increased adherence of the A909Δ*rodA* strain in the Caco-2 and
328 T84 cell lines compared to the A909 WT strain **(Figure 6A, B)**. In contrast, invasion assay
329 results differed by cell type. In Caco-2 cell, there was no difference in invasion between the
330 A909 WT and A909Δ*rodA* strains, whereas in T84 cells, there was an increase in invasion by the
331 A909Δ*rodA* strain **(Figure 6C, D)**. These findings suggest that the loss of *rodA* alters biofilm
332 responses to gastrointestinal stressors and increases epithelial adherence.

333 **Discussion**

334 The GBS cell wall is composed of a thick layer of peptidoglycan that anchors surface molecules
335 and consists of an outermost boundary of capsular polysaccharide that serves as a major factor in
336 colonization and pathogenesis (32-35). SEDS-family proteins, including RodA, are conserved
337 transmembrane enzymes that are key meditators of peptidoglycan synthesis and cell wall
338 integrity (36). RodA is a peptidoglycan polymerase that elongates glycan strands (16). It works
339 with PBP's, known to mediate peptide crosslinking, together playing a key morphogenetic role
340 in bacterial cell wall synthesis (37, 38). Studies in several enteric pathogens illustrate that

341 disruptions in glycan polymerization can have varying phenotypes depending on the organism
342 and the environmental niche (37, 39-44). Laubacher et al. demonstrated that peptidoglycan stress
343 activates Rcs envelope stress response in *E. coli*, leading to upregulation of capsule
344 polysaccharide genes and contributing to increased intrinsic resistance in the presence of
345 antibiotics (40). Prior reports have shown that the deletion of *rodA* leads to a loss of structure as
346 seen in *Streptococcus pneumoniae*, *E. coli*, and *Bacillus subtilis* (39, 41, 44, 45). In contrast, our
347 Δ*rodA* mutant showed no obvious changes to the bacterial shape by TEM and retained its
348 capsular expression. This phenotypic difference from other bacteria may reflect species-specific
349 differences in peptidoglycan synthesis or the relative contribution of RodA to overall cell wall
350 integrity. In addition, as previously described in *Bacillus subtilis*, mechanisms such as alternative
351 PG polymerases may compensate for the overall peptidoglycan integrity in GBS in the absence
352 of RodA (37). Structural characterization also revealed a chaining/aggregating effect by
353 A909Δ*rodA* on Gram staining. We propose that the aggregating and chaining phenomenon are
354 due to subtle changes in peptidoglycan remodeling rather than a direct defect in division or
355 capsule synthesis.

356 We noted increased adherence by the A909Δ*rodA* strain to both Caco-2 and T84 cell lines which
357 may be driven by the pronounced chaining/aggregating phenotype. The difference in cell type
358 specific responses to invasion, higher in the T84 than the Caco-2 cell line, may reflect specific
359 characteristics of the host epithelial surface, including mucus production or barrier integrity.
360 These results differ from *Salmonella*, where disruption of RodA-PBP complexes downregulates
361 classical invasion factors such as flagella, which could imply that RodA modulates host
362 interactions by physical rather than regulatory interactions (42). The biological significance of
363 increased adherence with varied invasion in the mutant strain remain unclear and may reflect

364 differences in morphological architecture of the epithelial cell lines, where Caco-2 cell line is
365 known to show a distinct biochemical signature of mature small intestinal enterocytes whereas
366 the T84 cell line retains its colonic differentiation (46).

367 In a model of GI colonization, we noted that the A909Δ*rodA* mutant displayed adequate
368 colonization during monocolonization but was significantly outcompeted by the WT strain
369 during cocolonization. We noted comparable bacterial burden across different sites of the GI
370 tract, except the colon, in longitudinal experiments. This suggests that *rodA* is not essential for
371 intestinal colonization but may confer an advantage under competitive pressure. This
372 phenomenon of competitive interactions has been described in other enteric pathogens and is
373 likely dependent on host, microbial, or nutritional pressures that become apparent during
374 competition (47-49).

375 Exposure to intestinal physiological stressors like acid, bile and lysozyme showed that *rodA* is
376 important for bile tolerance and biofilm adaptation to certain stressors. Jia et al. reported the
377 conditional essentiality of the *rodA* gene to bile salt resistance by GBS (17). We hypothesize that
378 the absence of *rodA* may impact the ability of the bacteria to polymerize glycan strands making
379 the cell wall more permeable. This could explain the increase in bile susceptibility which
380 disrupts the bacterial cell envelope by causing cell membrane leakage and denaturing proteins.
381 Interestingly, the A909Δ*rodA* mutant showed greater susceptibility at 0.5% bile concentration
382 compared to 1% bile concentration which was not seen in the A909 WT strain. This may indicate
383 differential compensatory response of the A909Δ*rodA* mutant cell wall to bile and warrants
384 further investigation. The reduced viability of GBS in short term assays but absence of long-term
385 growth defect on lysozyme exposure, may reflect bacterial killing with subsequent recovery of
386 surviving cells or obscuring of early CFU loss due to OD_{600} measurements (50). We also noted

387 WT GBS increased biofilm formation in response to lysozyme, consistent with stress-induced
388 biofilm formation described in other Gram-positive bacteria (51, 52). The absence of this
389 response in the Δ*rodA* mutant suggests that RodA contributes to envelope remodeling under
390 host-derived stress.

391 The context-dependent role of RodA uncovered in this report reflects its biological relevance
392 under stress/competition as well as its conditional requirement for envelope integrity. RodA
393 permits GBS to withstand physiological stressors, particularly bile, and to compete in the GI
394 tract. It gives us a window into the dynamic microbial changes that occur in a natural setting
395 during colonization persistence and/or clearance. This work highlights the importance of
396 identifying other conditionally essential genes like *rodA* that confer a competitive advantage in
397 the GI tract to inform strategies to disrupt GBS colonization.

398 **ACKNOWLEDGMENTS**

399 **Funding.** This work was supported by grant R01AI155476 to A.J.R. The content is solely the
400 responsibility of the authors and does not necessarily represent the official views of the funding
401 bodies. We thank NYULH Microscopy Lab (partially supported by NYU Cancer Center Support
402 Grant NIH/NCI P30CA016087) for consultation and preparation of the electron microscopy
403 images.

404 **Potential conflicts of interest.** The authors declare that they have no conflicts of interest.

405 **Author Notes.** This work was presented in part at the Pediatric Academic Societies' 2025
406 Annual Meeting.

407

408 **References**

409 1. Malvolti S, Pecenka C, Mantel CF, Malhame M, Lambach P. 2022. A Financial and
410 Global Demand Analysis to Inform Decisions for Funding and Clinical Development of
411 Group B *Streptococcus* Vaccines for Pregnant Women. Clin Infect Dis 74:S70-S79.
412 2. Puopolo KM, Lynfield R, Cummings JJ, Committee On Fetus And Newborn; Committee
413 On Infectious Diseases. 2019. Management of Infants at Risk for Group B Streptococcal
414 Disease. Pediatrics 144: e20191881.
415 3. Nanduri SA, Petit S, Smelser C, Apostol M, Alden NB, Harrison LH, Lynfield R,
416 Vagnone PS, Burzlaff K, Spina NL, Dufort EM, Schaffner W, Thomas AR, Farley MM,
417 Jain JH, Pondo T, McGee L, Beall BW, Schrag SJ. 2019. Epidemiology of Invasive
418 Early-Onset and Late-Onset Group B Streptococcal Disease in the United States, 2006 to
419 2015: Multistate Laboratory and Population-Based Surveillance. JAMA Pediatr 173:224-
420 233.
421 4. Centers for Disease Control and Prevention. 2023. Active bacterial core surveillance
422 report, emerging infections program network, Group B *Streptococcus*, 2023.
423 https://www.cdc.gov/abcs/downloads/GBS_Surveillance_Report_2023.pdf. Accessed 20
424 September 2025.
425 5. Karampatsas K, Davies H, Mynarek M, Andrews N, Heath PT, Le Doare K. 2022.
426 Clinical Risk Factors Associated With Late-Onset Invasive Group B Streptococcal
427 Disease: Systematic Review and Meta-Analyses. Clin Infect Dis 75:1255-1264.
428 6. Puopolo KM, Mukhopadhyay S, Hansen NI, Flannery DD, Greenberg RG, Sanchez PJ,
429 Bell EF, DeMauro SB, Wyckoff MH, Eichenwald EC, Stoll BJ. 2022. Group B
430 *Streptococcus* Infection in Extremely Preterm Neonates and Neurodevelopmental
431 Outcomes at 2 Years. Clin Infect Dis 75:1405-1415.
432 7. Madrid L, Seale AC, Kohli-Lynch M, Edmond KM, Lawn JE, Heath PT, Madhi SA,
433 Baker CJ, Bartlett L, Cutland C, Gravett MG, Ip M, Le Doare K, Rubens CE, Saha SK,
434 Sobanjo-Ter Meulen A, Vekemans J, Schrag S, nfant GBS Disease Investigator Group.
435 2017. Infant Group B Streptococcal Disease Incidence and Serotypes Worldwide:
436 Systematic Review and Meta-analyses. Clin Infect Dis 65:S160-S172.
437 8. Berardi A, Lugli L, Rossi C, China MC, Vellani G, Contiero R, Calanca F, Camerlo F,
438 Casula F, Di Carlo C, Rossi MR, Chiarabini R, Ferrari M, Minniti S, Venturelli C,
439 Silvestrini D, Dodi I, Zucchini A, Ferrari F, Infezioni da Streptococco B Della Regione
440 Emilia Romagna. 2010. Neonatal bacterial meningitis. Minerva Pediatr 62:51-54.
441 9. Libster R, Edwards KM, Levent F, Edwards MS, Rench MA, Castagnini LA, Cooper T,
442 Sparks RC, Baker CJ, Shah PE. 2012. Long-term outcomes of group B streptococcal
443 meningitis. Pediatrics 130:e8-15.
444 10. Kohli-Lynch M, Russell NJ, Seale AC, Dangor Z, Tann CJ, Baker CJ, Bartlett L, Cutland
445 C, Gravett MG, Heath PT, Ip M, Le Doare K, Madhi SA, Rubens CE, Saha SK, Schrag S,
446 Sobanjo-Ter Meulen A, Vekemans J, O'Sullivan C, Nakwa F, Ben Hamouda H, Soua H,
447 Giorgakoudi K, Ladhani S, Lamagni T, Rattue H, Trotter C, Lawn JE. 2017.
448 Neurodevelopmental Impairment in Children After Group B Streptococcal Disease
449 Worldwide: Systematic Review and Meta-analyses. Clin Infect Dis 65:S190-S199.
450 11. Goncalves BP, Procter SR, Paul P, Chandna J, Lewin A, Seedat F, Koukounari A,
451 Dangor Z, Leahy S, Santhanam S, John HB, Bramugy J, Bardaji A, Abubakar A,
452 Nasambu C, Libster R, Sanchez Yanotti C, Horvath-Puho E, Sorensen HT, van de Beek

453 D, Bijlsma MW, Gardner WM, Kassebaum N, Trotter C, Bassat Q, Madhi SA, Lambach
454 P, Jit M, Lawn JE, GBS Danish and Dutch collaborative group for long term outcomes;
455 GBS Low and Middle Income Countries collaborative group for long term outcomes;
456 GBS Scientific Advisory Group, epidemiological sub-group; CHAMPS team. 2022.
457 Group B *streptococcus* infection during pregnancy and infancy: estimates of regional and
458 global burden. Lancet Glob Health 10:e807-e819.
459 12. Carl MA, Ndao IM, Springman AC, Manning SD, Johnson JR, Johnston BD, Burnham
460 CA, Weinstock ES, Weinstock GM, Wylie TN, Mitreva M, Abubucker S, Zhou Y,
461 Stevens HJ, Hall-Moore C, Julian S, Shaikh N, Warner BB, Tarr PI. 2014. Sepsis from
462 the gut: the enteric habitat of bacteria that cause late-onset neonatal bloodstream
463 infections. Clin Infect Dis 58:1211-1218.
464 13. Schwartz DJ, Shalon N, Wardenburg K, DeVeaux A, Wallace MA, Hall-Moore C, Ndao
465 IM, Sullivan JE, Radmacher P, Escobedo M, Burnham CD, Warner BB, Tarr PI, Dantas
466 G. 2023. Gut pathogen colonization precedes bloodstream infection in the neonatal
467 intensive care unit. Sci Transl Med 15:eadg5562.
468 14. Vaz MJ, Purrier SA, Bonakdar M, Chamby AB, Ratner AJ, Randis TM. 2020. The
469 Impact of Circulating Antibody on Group B *Streptococcus* Intestinal Colonization and
470 Invasive Disease. Infect Immun 89:e00348-20.
471 15. Zhu L, Yerramilli P, Pruitt L, Mishra A, Olsen RJ, Beres SB, Waller AS, Musser JM.
472 2021. Functional Insights into the High-Molecular-Mass Penicillin-Binding Proteins of
473 *Streptococcus agalactiae* Revealed by Gene Deletion and Transposon Mutagenesis
474 Analysis. J Bacteriol 203:e0023421.
475 16. Welsh MA, Schaefer K, Taguchi A, Kahne D, Walker S. 2019. Direction of Chain
476 Growth and Substrate Preferences of Shape, Elongation, Division, and Sporulation-
477 Family Peptidoglycan Glycosyltransferases. J Am Chem Soc 141:12994-12997.
478 17. Jia L, Yuan C, Pan F, Zhou X, Fan H, Ma Z. 2023. CsbD, a Novel Group B Streptococcal
479 Stress Response Factor That Contributes to Bacterial Resistance against Environmental
480 Bile Salts. J Bacteriol 205:e0044822.
481 18. Hillebrand GH, Carlin SC, Giacobe EJ, Stephenson HA, Collins J, Hooven TA. 2025. A
482 Cas12a Toolbox for Rapid and Flexible Group B *Streptococcus* Genomic Editing and
483 CRISPRi. Mol Microbiol doi:10.1111/mmi.70022.
484 19. Nunez Pedrozo CN, Peralta TM, Olea FD, Locatelli P, Crottogini AJ, Belaich MN,
485 Cuniberti LA. 2022. In silico performance analysis of web tools for CRISPRa sgRNA
486 design in human genes. Comput Struct Biotechnol J 20:3779-3782.
487 20. Helle L, Kull M, Mayer S, Marincola G, Zelder ME, Goerke C, Wolz C, Bertram R.
488 2011. Vectors for improved Tet repressor-dependent gradual gene induction or silencing
489 in *Staphylococcus aureus*. Microbiology (Reading) 157:3314-3323.
490 21. Bhavana VH, Hillebrand GH, Gopalakrishna KP, Rapp RA, Ratner AJ, Tettelin H,
491 Hooven TA. 2023. A group B *Streptococcus* indexed transposon mutant library to
492 accelerate genetic research on an important perinatal pathogen. Microbiol Spectr
493 11:e0204623.
494 22. Moyes RB, Reynolds J, Breakwell DP. 2009. Differential staining of bacteria: gram stain.
495 Curr Protoc Microbiol Appendix 3:Appendix 3C.
496 23. Hammerschmidt S, Wolff S, Hocke A, Rosseau S, Muller E, Rohde M. 2005. Illustration
497 of pneumococcal polysaccharide capsule during adherence and invasion of epithelial
498 cells. Infect Immun 73:4653-4667.

499 24. Vaz MJ, Dongas S, Ratner AJ. 2023. Capsule production promotes Group B
500 *Streptococcus* intestinal colonization. Microbiol Spectr 11:e0234923.
501 25. Yang Q, Porter AJ, Zhang M, Harrington DJ, Black GW, Sutcliffe IC. 2012. The impact
502 of pH and nutrient stress on the growth and survival of *Streptococcus agalactiae*. Antonie
503 Van Leeuwenhoek 102:277-287.
504 26. Patras KA, Derieux J, Al-Bassam MM, Adiletta N, Vrbanac A, Lapek JD, Zengler K,
505 Gonzalez DJ, Nizet V. 2018. Group B *Streptococcus* Biofilm Regulatory Protein A
506 Contributes to Bacterial Physiology and Innate Immune Resistance. J Infect Dis
507 218:1641-1652.
508 27. D'Urzo N, Martinelli M, Pezzicoli A, De Cesare V, Pinto V, Margarit I, Telford JL,
509 Maione D, Members of the DSG. 2014. Acidic pH strongly enhances in vitro biofilm
510 formation by a subset of hypervirulent ST-17 *Streptococcus agalactiae* strains. Appl
511 Environ Microbiol 80:2176-2185.
512 28. De Gaetano GV, Lentini G, Galbo R, Coppolino F, Fama A, Teti G, Beninati C. 2021.
513 Invasion and trafficking of hypervirulent group B streptococci in polarized enterocytes.
514 PLoS One 16:e0253242.
515 29. Dominguez K, Pearah AN, Lindon AK, Worthington LA, Carter RR, John-Lewis
516 Edwards N, Ho TTB, Darch SE, Randis TM. 2024. The impact of butyrate on group B
517 *Streptococcus*-induced intestinal barrier disruption. Infect Immun 92:e0020024.
518 30. Yang Q, Li N, Zheng Y, Tian Y, Liang Q, Zhao M, Chu H, Gong Y, Wu T, Wei S, Wang
519 H, Yan G, Li F, Lei L. 2025. Identification and characterization of *ugpE* associated with
520 the full virulence of *Streptococcus suis*. Vet Res 56:82.
521 31. Baron MJ, Kasper DL. 2005. Anchors away: contribution of a glycolipid anchor to
522 bacterial invasion of host cells. J Clin Invest 115:2325-2327.
523 32. Silhavy TJ, Kahne D, Walker S. 2010. The bacterial cell envelope. Cold Spring Harb
524 Perspect Biol 2:a000414.
525 33. Wessels MR, Rubens CE, Benedi VJ, Kasper DL. 1989. Definition of a bacterial
526 virulence factor: sialylation of the group B streptococcal capsule. Proc Natl Acad Sci U S
527 A 86:8983-8987.
528 34. Rosini R, Margarit I. 2015. Biofilm formation by *Streptococcus agalactiae*: influence of
529 environmental conditions and implicated virulence factors. Front Cell Infect Microbiol
530 5:6.
531 35. Kampff Z, van Sinderen D, Mahony J. 2023. Cell wall polysaccharides of streptococci: A
532 genetic and structural perspective. Biotechnol Adv 69:108279.
533 36. Meeske AJ, Riley EP, Robins WP, Uehara T, Mekalanos JJ, Kahne D, Walker S, Kruse
534 AC, Bernhardt TG, Rudner DZ. 2016. SEDS proteins are a widespread family of
535 bacterial cell wall polymerases. Nature 537:634-638.
536 37. Emami K, Guyet A, Kawai Y, Devi J, Wu LJ, Allenby N, Daniel RA, Errington J. 2017.
537 RodA as the missing glycosyltransferase in *Bacillus subtilis* and antibiotic discovery for
538 the peptidoglycan polymerase pathway. Nat Microbiol 2:16253.
539 38. Cho H, Wivagg CN, Kapoor M, Barry Z, Rohs PDA, Suh H, Marto JA, Garner EC,
540 Bernhardt TG. 2016. Bacterial cell wall biogenesis is mediated by SEDS and PBP
541 polymerase families functioning semi-autonomously. Nat Microbiol 1:16172.
542 39. Ranjit DK, Young KD. 2013. The Rcs stress response and accessory envelope proteins
543 are required for de novo generation of cell shape in *Escherichia coli*. J Bacteriol
544 195:2452-2462.

545 40. Laubacher ME, Ades SE. 2008. The Rcs phosphorelay is a cell envelope stress response
546 activated by peptidoglycan stress and contributes to intrinsic antibiotic resistance. J
547 Bacteriol 190:2065-2074.
548 41. Bendezu FO, Hale CA, Bernhardt TG, de Boer PA. 2009. RodZ (*YfgA*) is required for
549 proper assembly of the MreB actin cytoskeleton and cell shape in *E. coli.* EMBO J
550 28:193-204.
551 42. Doble AC, Clark-Corrigall J, Bulmer DM, Daniel RA, Mastroeni P, Anjam Khan CM.
552 2024. Essential roles of RodA peptidoglycan polymerase and PBP2 transpeptidase in
553 expression of cell wall-spanning supramolecular organelles and
554 modulating *Salmonella* virulence. bioRxiv [Preprint]. doi:10.1101/2024.07.01.601524.
555 43. Arora D, Chawla Y, Malakar B, Singh A, Nandicoori VK. 2018. The transpeptidase
556 PbpA and noncanonical transglycosylase RodA of *Mycobacterium tuberculosis* play
557 important roles in regulating bacterial cell lengths. J Biol Chem 293:6497-6516.
558 44. Lamanna MM, Manzoor I, Joseph M, Ye ZA, Benedet M, Zanardi A, Ren Z, Wang X,
559 Massidda O, Tsui HT, Winkler ME. 2022. Roles of RodZ and class A PBP1b in the
560 assembly and regulation of the peripheral peptidoglycan elongasome in ovoid-shaped
561 cells of *Streptococcus pneumoniae* D39. Mol Microbiol 118:336-368.
562 45. Henriques AO, Glaser P, Piggot PJ, Moran CP, Jr. 1998. Control of cell shape and
563 elongation by the rodA gene in Bacillus subtilis. Mol Microbiol 28:235-47.
564 46. Devriese S, Van den Bossche L, Van Welden S, Holvoet T, Pinheiro I, Hindryckx P, De
565 Vos M, Laukens D. 2017. T84 monolayers are superior to Caco-2 as a model system of
566 colonocytes. Histochem Cell Biol 148:85-93.
567 47. Li SH, Li Z, Park JO, King CG, Rabinowitz JD, Wingreen NS, Gitai Z. 2018.
568 *Escherichia coli* translation strategies differ across carbon, nitrogen and phosphorus
569 limitation conditions. Nat Microbiol 3:939-947.
570 48. Liu H, Shiver AL, Price MN, Carlson HK, Trotter VV, Chen Y, Escalante V, Ray J, Hern
571 KE, Petzold CJ, Turnbaugh PJ, Huang KC, Arkin AP, Deutschbauer AM. 2021.
572 Functional genetics of human gut commensal *Bacteroides thetaiotaomicron* reveals
573 metabolic requirements for growth across environments. Cell Rep 34:108789.
574 49. Stubbendieck RM, May DS, Chevrette MG, Temkin MI, Wendt-Pienkowski E, Cagnazzo
575 J, Carlson CM, Gern JE, Currie CR. 2019. Competition among Nasal Bacteria Suggests a
576 Role for Siderophore-Mediated Interactions in Shaping the Human Nasal Microbiota.
577 Appl Environ Microbiol 85:e00637-19.
578 50. Stevenson K, McVey AF, Clark IBN, Swain PS, Pilizota T. 2016. General calibration of
579 microbial growth in microplate readers. Sci Rep 6:38828.
580 51. Rouchon CN, Harris J, Zubair-Nizami Z, Weinstein AJ, Roky M, Frank KL. 2022. The
581 Cationic Antimicrobial Peptide Activity of Lysozyme Reduces Viable *Enterococcus*
582 *faecalis* Cells in Biofilms. Antimicrob Agents Chemother 66:e0233921.
583 52. Grimm I, Dumke J, Dreier J, Knabbe C, Vollmer T. 2018. Biofilm formation and
584 transcriptome analysis of *Streptococcus gallolyticus* subsp. *gallolyticus* in response to
585 lysozyme. PLoS One 13:e0191705.
586

587

588 **Figure Legends**

589 **Figure 1. Structural characterization of WT and *rodA* deficient GBS. A**. Gram-stained
590 images of A909 WT and A909Δ*rodA* strains in stationary growth, taken at 63×original
591 magnification. Scale bar = 5 µm. Experiments were performed twice independently, with
592 representative images shown. **B.** Capsule production assessed by colony immunoblot using a
593 serotype Ia-specific anti-capsular polysaccharide antibody in A909 WT, A909Δ*cpsE* (acapsular
594 control) and A909Δ*rodA* strains. Positive: Halo around brown colonies; Negative: brown
595 colonies only. Representative blot from two independent experiments is shown. **C.** Latex
596 agglutination was used to confirm production of capsule. Type Ia antisera was used for A909
597 WT, A909 Δ*cpsE* (acapsular control) and A909Δ*rodA* strains. Positive: clumping noted;
598 Negative: no clumping noted. Representative images from two independent experiments are
599 shown. **D.** Transmission electron microscopy demonstrates capsule and cell wall in A909 WT
600 and A909Δ*rodA* strains. Bacteria were chemically fixed by including lysine acetate during the
601 glutaraldehyde and formaldehyde exposure. Samples were stained and postfixed using
602 Ruthenium red and osmium and subsequently embedded in LR White. Black arrows mark the
603 capsule, and white arrows mark the cell wall. Scale bar = 200 nm. Representative images from
604 10 fields per strains are shown.

605 **Figure 2. RodA confers a competitive advantage to GBS in an intestinal colonization**
606 **competition model.** Preweaning C57BL/6J mice were orally inoculated with a 1:1 mixture of
607 A909 WT and A909Δ*rodA* in an experimental cohort (n = 5). **A.** Kaplan-Meier survival curve
608 demonstrates 100% survival. **B.** The small intestine, cecum, and colon, were harvested at 7 days
609 post inoculation. Approximately 100 colonies per GI site (~20 colonies per mouse) were

610 analyzed using cPCR to differentiate between A909 WT and A909Δ*rodA*. Data points represent
611 geometric mean competition indices and error bars represent 95% confidence intervals.

612 **Figure 3. Comparable colonization by the A909Δ*rodA* mutant and A909 WT strains in**
613 **monocolonization.** Preweaning C57BL/6J mice were orally infected with either A909 WT or
614 A909Δ*rodA* in six separate cohorts, and the small intestine, cecum, and colon, were harvested at
615 predetermined time intervals. **A, B, C.** Percent colonization as determined by the presence of
616 GBS on days 3, 7, and 14 respectively (P = not significant [NS]; two-sided Fisher's exact test).
617 **D, E, F.** Bacterial burden determined as GBS CFU/gram tissue on days 3, 7, and 14 respectively.
618 Individual points represent biological replicates and lines showing median with interquartile
619 range, (*, $p<0.01$; **, $p<0.001$; two-way repeated measures ANOVA with Sidak's multiple
620 comparisons post-test). Sample sizes: A909 WT=4, A909Δ*rodA*=7 **(Figure A, D)**, A909 WT =
621 5, A909Δ*rodA* = 7 **(Figure B, E)**, A909 WT=4, A909Δ*rodA* = 6 **(Figure C, F)**.

622 **Figure 4. Exposure to intestinal physiological stressors reveals selective susceptibility of**
623 **A909Δ*rodA*.** Overnight cultures of A909 WT, A909Δ*rodA* and A909Δ*rodA*+pGBScomp
624 High::*rodA* GBS strains were diluted to an OD value of 0.05 in Todd-Hewitt broth and incubated
625 at 37°C. OD_{600} was measured at 20-minute intervals under different intestinal stressors. **A.**
626 Standard media (pH 7.34), **B.** Standard media, pH 6.0, **C.** Standard media, pH 5.0, **D.** Standard
627 media, bile 5 mg/ml (0.5%), **E**. Standard media, bile 10 mg/ml (1.0%), **F.** Standard media,
628 lysozyme 14 mg/ml. Data from independent samples (n = 9) with three technical replicates
629 shown, with lines indicating mean values ± standard errors of the mean (SEM).

630 **Figure 5. GBS *rodA* deficiency impacts biofilm formation under select stressor exposure.**
631 Biofilm formation of A909 WT and A909Δ*rodA* strains quantified by crystal violet uptake after

632 exposure to **A.** THB, with 1% glucose at pH 6.0, **B.** THB, with 1% glucose at pH 5.0, **C.** THB,
633 with 1% glucose, lysozyme 14 mg/ml, **D.** THB, with 1% glucose, bile 5 mg/ml, **E.** THB, with
634 1% glucose, bile 10 mg/ml. Data from independent samples (n = 9) with three technical
635 replicates are shown, and lines represent mean values ± SDs. Data were analyzed using two-way
636 ANOVA with the Tukey multiple comparisons test (*, $p<0.05$; **, $p<0.005$; ****$p< 0.0001$).

637 **Figure 6. The absence of *rodA* impacts adherence and differentially affects invasion in**
638 **intestinal epithelial cells. A, C.** Adhesion assays were performed with Caco-2 and T84
639 intestinal cell lines respectively at an MOI of 10. **B, D.** Invasion assays were performed with
640 Caco-2 and T84 intestinal cell lines respectively at an MOI 10. The percentage of adhered and
641 invaded bacteria were calculated relative to the initial inoculum. All data are from independent
642 experiments (n=9, each with 3 technical replicates). The error bars indicate the 95% confidence
643 intervals of the means of the wells. Data were analyzed using the Mann-Whitney U test (****, p
644 < 0.0001).

645

646

647

648

649

650

651

652

Figure 1

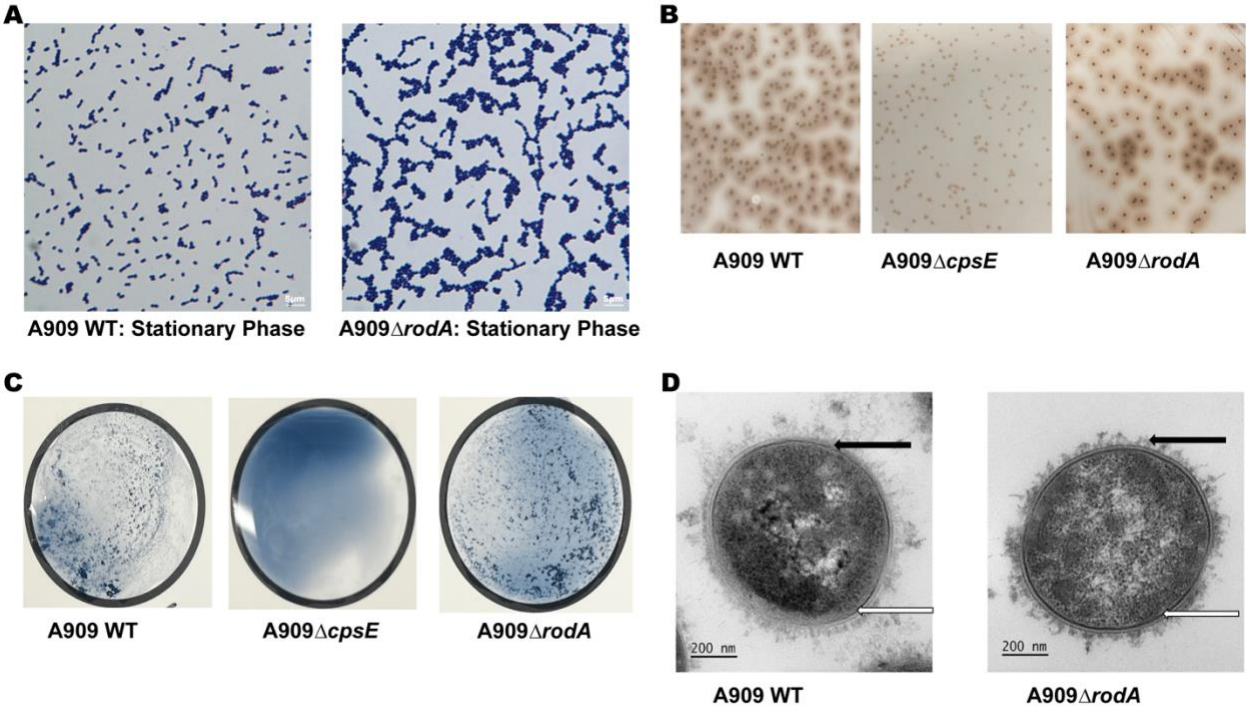

653

654

655

656

657

658

659
660
661
662
663
664
665

666
667
668
669

Figure 2

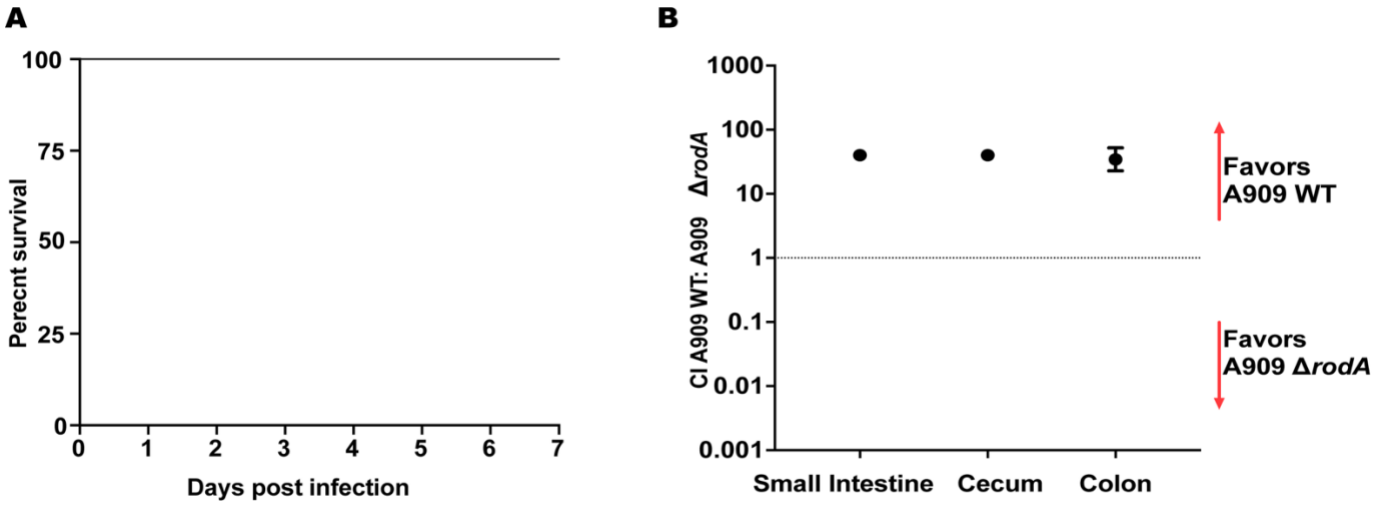

670
671
672
673
674
675
676
677
678
679
680
681
682
683
684
685
686
687
688
689
690
691
692
693
694
695

696
697

Figure 3

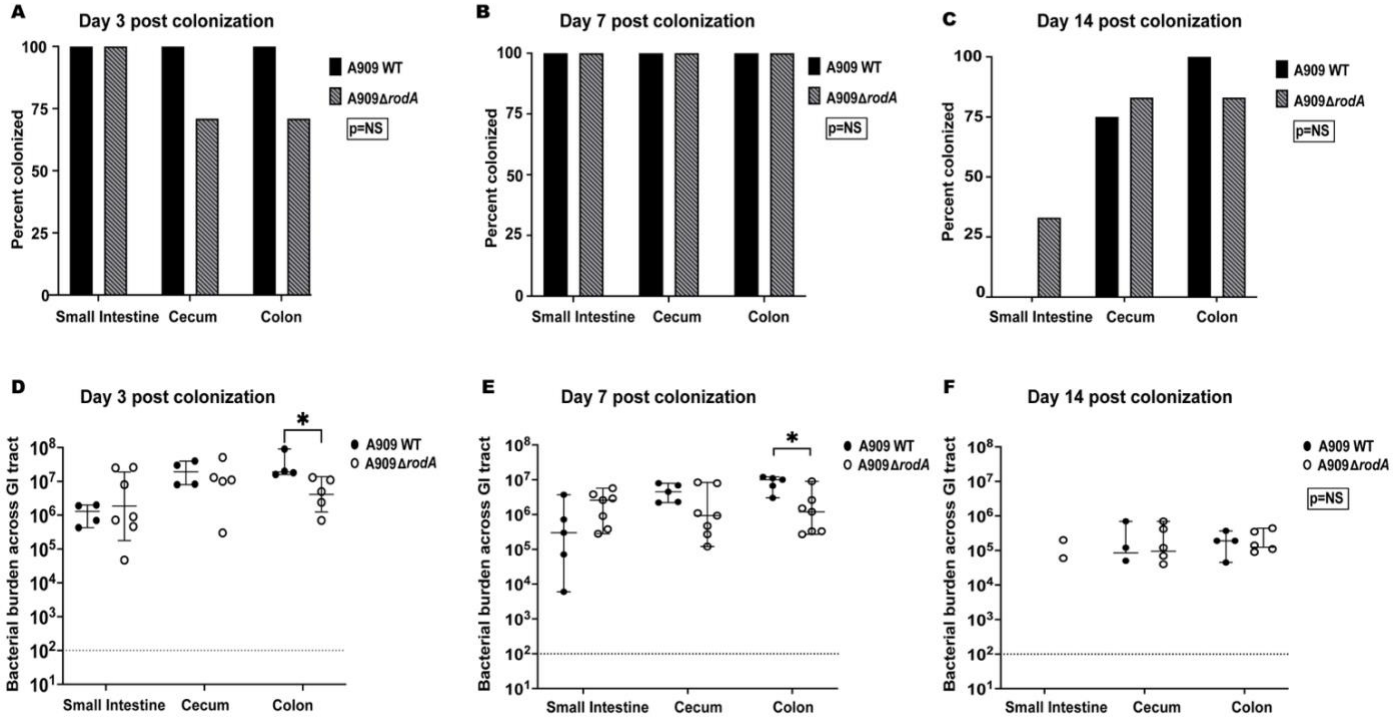

698
699
700
701
702
703
704
705
706
707
708

Figure 4

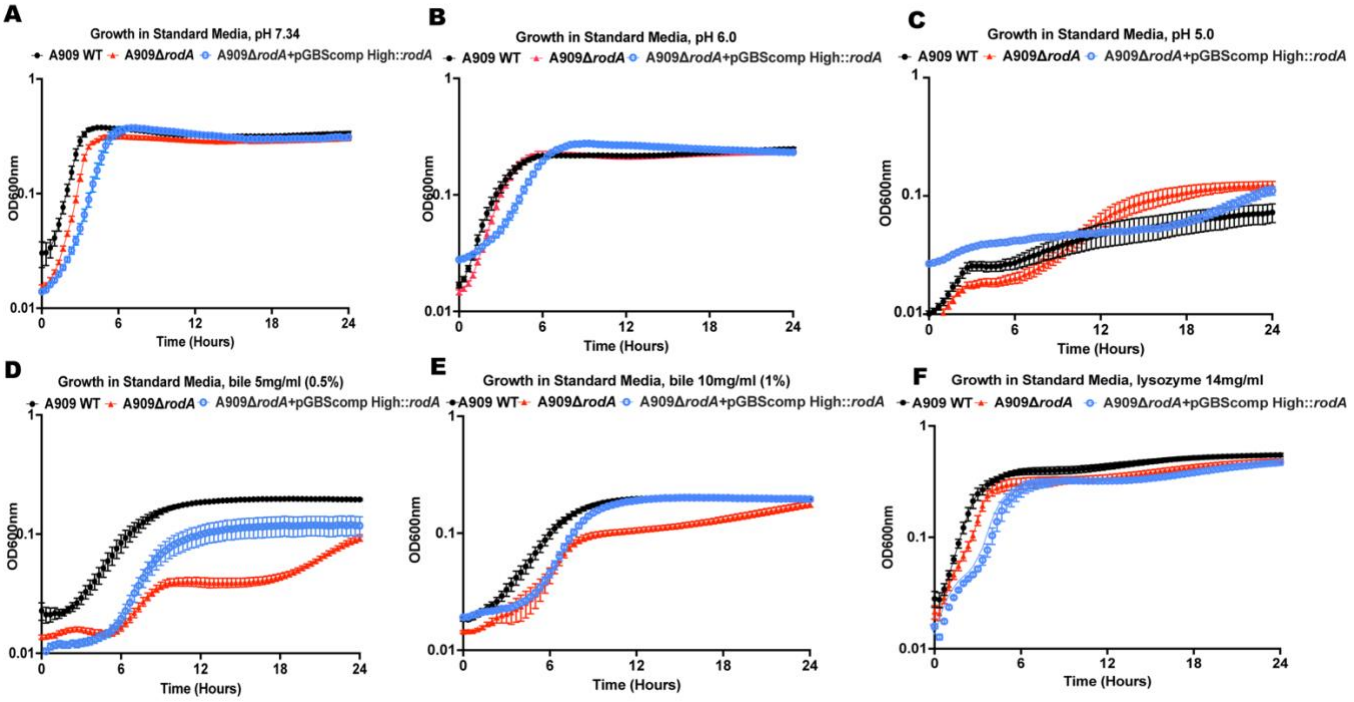
A
Growth in Standard Media, pH 7.34
A909 WT
A909ΔrodA
A909ΔrodA+pGBScomp High::rodA
OD600nm
Time (Hours)
B
Growth in Standard Media, pH 6.0
C
Growth in Standard Media, pH 5.0
D
Growth in Standard Media, bile 5mg/ml (0.5%)
E
Growth in Standard Media, bile 10mg/ml (1%)
F
Growth in Standard Media, lysozyme 14mg/ml

Figure 5

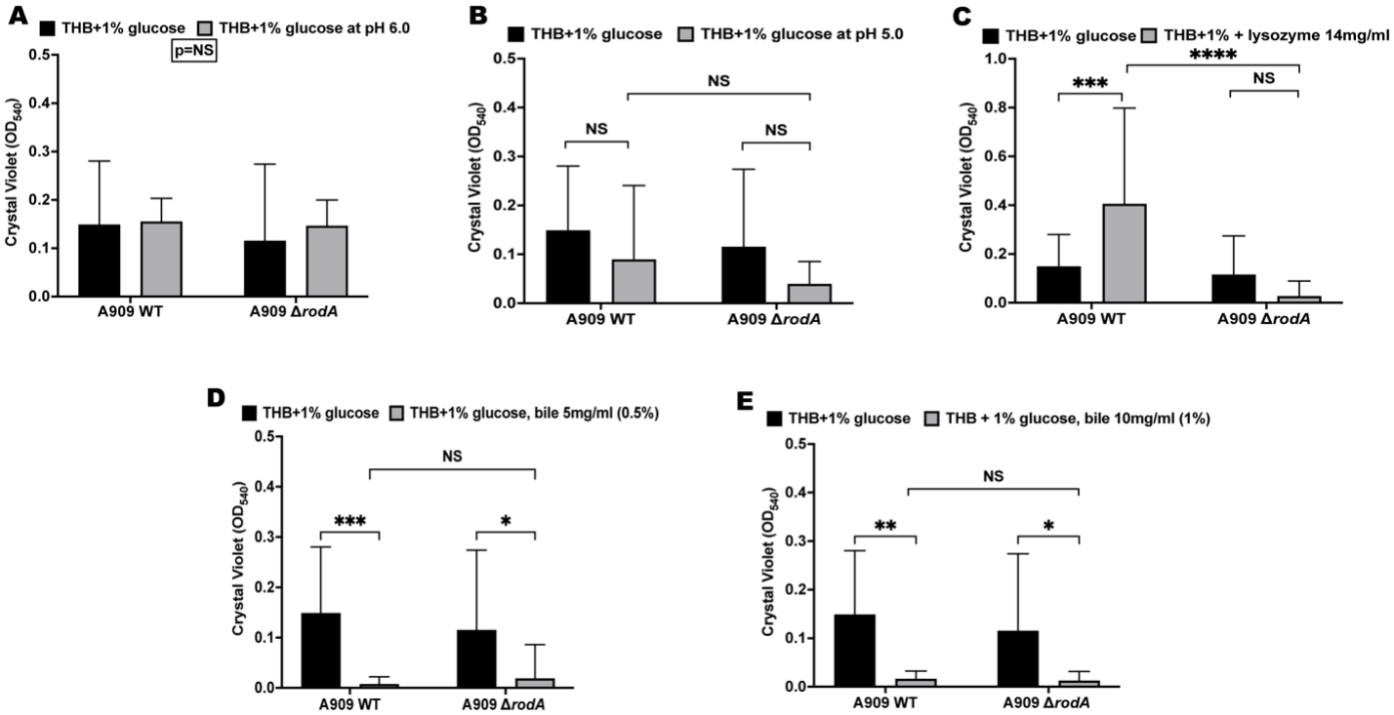
A
THB+1% glucose
THB+1% glucose at pH 6.0
p=NS
Crystal Violet (OD540)
0.5
0.4
0.3
0.2
0.1
0.0
A909 WT
A909 ΔrodA
B
THB+1% glucose
THB+1% glucose at pH 5.0
NS
NS
NS
Crystal Violet (OD540)
0.5
0.4
0.3
0.2
0.1
0.0
A909 WT
A909 ΔrodA
C
THB+1% glucose
THB+1% + lysozyme 14mg/ml
****
***
NS
Crystal Violet (OD540)
1.0
0.8
0.6
0.4
0.2
0.0
A909 WT
A909 ΔrodA
D
THB+1% glucose
THB+1% glucose, bile 5mg/ml (0.5%)
NS
***
*
Crystal Violet (OD540)
0.5
0.4
0.3
0.2
0.1
0.0
A909 WT
A909 ΔrodA
E
THB+1% glucose
THB + 1% glucose, bile 10mg/ml (1%)
NS
**
*
Crystal Violet (OD540)
0.5
0.4
0.3
0.2
0.1
0.0
A909 WT
A909 ΔrodA

Figure 6

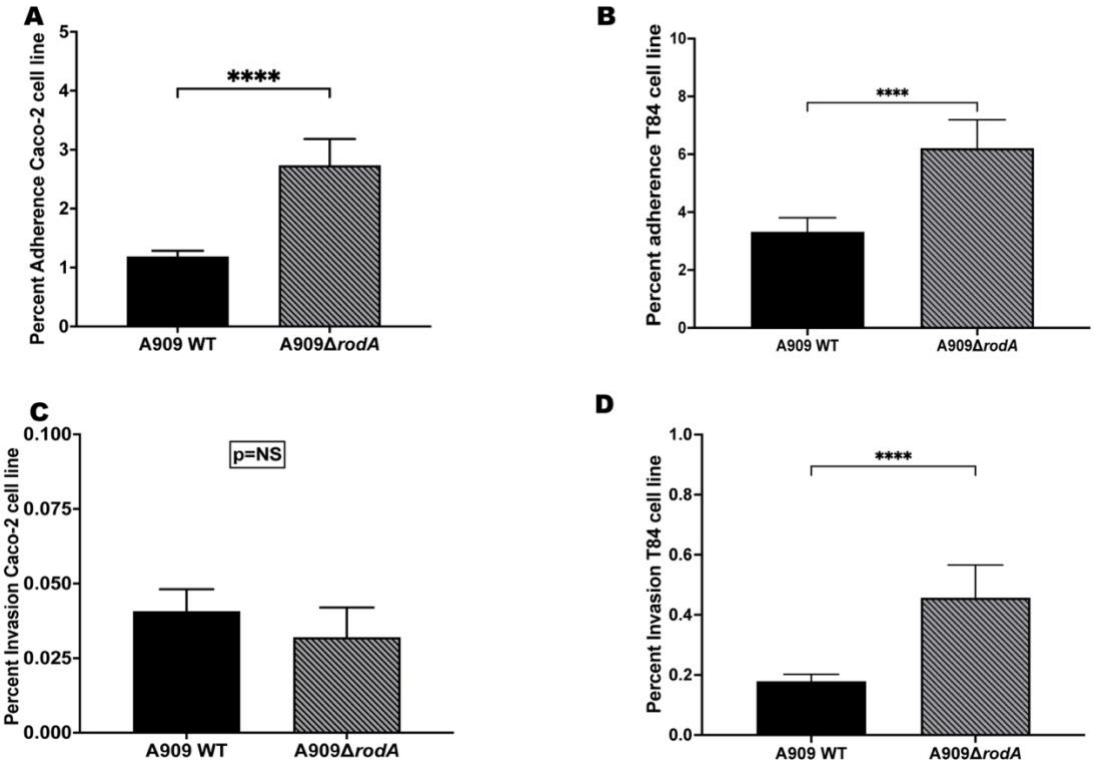

749

750

751